Low-cost space-varying FIR filter architecture for computational imaging systems

Guotong Feng[a], Mohammed Shoaib[b], Edward L. Schwartz[a] and M. Dirk Robinson[a]

[a]Ricoh Innovations Inc., 2882 Sand Hill Road, Suite 115, Menlo Park, California 94025, USA
[b]Department of Electrical Engineering, Princeton University, Princeton, New Jersey 08544, USA

ABSTRACT

Recent research demonstrates the advantage of designing electro-optical imaging systems by jointly optimizing the optical and digital subsystems. The optical systems designed using this joint approach intentionally introduce large and often space-varying optical aberrations that produce blurry optical images. Digital sharpening restores reduced contrast due to these intentional optical aberrations. Computational imaging systems designed in this fashion have several advantages including extended depth-of-field, lower system costs, and improved low-light performance. Currently, most consumer imaging systems lack the necessary computational resources to compensate for these optical systems with large aberrations in the digital processor. Hence, the exploitation of the advantages of the jointly designed computational imaging system requires low-complexity algorithms enabling space-varying sharpening.

In this paper, we describe a low-cost algorithmic framework and associated hardware enabling the space-varying finite impulse response (FIR) sharpening required to restore largely aberrated optical images. Our framework leverages the space-varying properties of optical images formed using rotationally-symmetric optical lens elements. First, we describe an approach to leverage the rotational symmetry of the point spread function (PSF) about the optical axis allowing computational savings. Second, we employ a specially designed bank of sharpening filters tuned to the specific radial variation common to optical aberrations. We evaluate the computational efficiency and image quality achieved by using this low-cost space-varying FIR filter architecture.

Keywords: Space-varying, sharpening, FIR, filter bank, optical aberrations, image rotation, FPGA, multiplexer arrays, joint electro-optical design, computational imaging systems

1. INTRODUCTION

Recent research demonstrates the advantages of designing electro-optical imaging systems by jointly optimizing the optical and digital processing sub-systems. In conventional optical system design methodologies, the goal has been the minimization of optical aberrations. On the contrary, optical systems designed using the new joint approach intentionally introduce larger aberrations by incorporating low-cost optical components that consequently produce more blurry optical images. Further, the new approach entails subsequent digital sharpening to restore reduced contrast due to these intentional optical aberrations. Computational imaging systems designed in this fashion provide several system-level advantages including extended depth-of-field, lower system costs, and improved low-light performance.[1–4] The optical aberrations of such imaging systems, however, are typically large and often space-varying.[5] Hence the exploitation of the advantages of these systems raises a demanding challenge on digital image processing. Currently, most consumer imaging systems lack the necessary computational resources to compensate for these optical sub-systems with large aberrations. In such a scenario, achieving a jointly designed electro-optical imaging system requires low-complexity algorithms and high-efficiency hardware architectures. More specifically, space-varying digital filters emerge as major enablers for such processing needs.

In the literature, the implementation of space-varying filters in software has been extensively studied, astronomy being one of the application areas.[6] A number of algorithms for space-varying filters, modulation transfer function (MTF) compensation, or deblurring have been proposed to improve the performance (typically speed of computation).[7–11] These

† Further author information: (Send correspondence to Guotong Feng)
Guotong Feng: *E-mail*: feng@rii.ricoh.com, Telephone: 1 650 496 5715
Mohammed Shoaib: *E-mail*: mshoaib@princeton.edu, Telephone: 1 609 613 2833
M. Dirk Robinson: *E-mail*: dirkr@rii.ricoh.com, Telephone: 1 650 496 5703

algorithms employ fast iterative methods, or fast matrix-vector products using linear interpolation. Many other approaches have focussed on motion blur correction by coordinate transformations using mechanical motion models,[12] sectional processing,[13,14] and iterative methods.[15] The coordinate transformation approach[12] transforms the linear shift (space) variant (LSV) system to linear shift invariant (LSI) degradation and in the sectioning methods, the image is sectioned into regions, where each section is restored using a separate space-invariant deblurring filter stored in memory. The mapping approach directs an iteratively designed maximum aposteriori filter[15] or other variations based on a decision-based algorithm. However, the complexity and memory requirements of these algorithms make them impractical for low-cost hardware implementation.

In this paper, we describe a low-cost algorithmic framework and associated hardware architecture for the joint design approach enabling the space-varying image sharpening required to restore the aberrated optical images. Our framework leverages the space-varying properties of optical images formed using rotationally symmetric optical lenses. First, we describe a low-cost approach, which we call space-varying rotation based finite impulse response (FIR) filter architecture, to leverage the rotational symmetry of the point spread function (PSF) about the optical axis. This architecture works by rotating an input image patch centered at the current pixel being processed by a certain angle and then performing FIR sharpening on the rotated image patch. The rotation angle depends on the location of the current pixel in a small set of angular tiles that are uniformly segmented across the image. This approach takes the advantage of the rotational properties of FIR filters along the angular direction by using a low-cost multi-stage binary multiplexer network for image patch rotation. Secondly, we employ a specially designed bank of sharpening filters to leverage the radial variation common to optical aberrations. The filter bank consists of a set of 2-D FIR sharpening filters, each of which is applied to the same rotated input image patch. The outputs of the FIR filters are linearly combined using a set of weights to produce the final filtered output for the current pixel under process. The weight for each FIR filter output is a function of the current pixel radius, which is dependent on the radial variation in the optical PSFs. We evaluate the computational efficiency in hardware using the proposed low-cost algorithmic framework. We also show simulation results demonstrating the image quality achieved by using our novel space-varying FIR filter architecture.

The rest of this paper is organized as follows. Section 2 presents the approximation model of space-varying filtering that underlies the proposed architecture. Section 3 explains the details of the space-varying rotation based FIR filter bank architecture. Section 4 describes the hardware implementation on a low-end field-programmable gate array (FPGA) platform. Section 5 shows some experimental results reflecting the cost and performance of the proposed architecture, and finally, Section 6 makes conclusions.

2. APPROXIMATION MODEL OF LINEAR SPACE-VARYING FILTERING

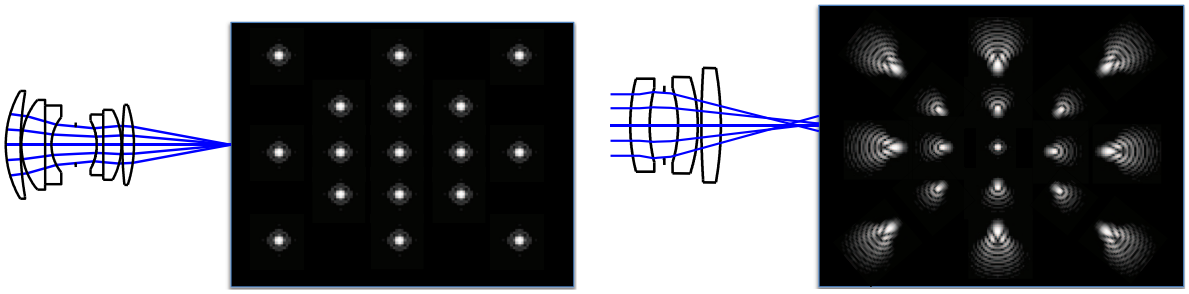

(a) (b)

Figure 1. The diagram shows two example optical systems with different field aberrations and the associated PSFs. The system in (a) has small field aberrations and the corresponding space-invariant PSFs. The system in (b) has large field aberrations and the corresponding space-varying PSFs. The PSFs have large variations along the radius, but are rotationally symmetric about the optical center.

Figure 1 shows two example optical systems with different field aberrations and the associated PSFs. The system in a) has small field aberrations and the corresponding space-invariant PSFs. The system in b) has large field aberrations and the corresponding space-varying PSFs. The PSFs have large variations along the radius, but are rotationally symmetric about the optical center. For digital correction of these aberrations, the system in a) only requires a single space-invariant filter to achieve desirable image quality, whereas the system in b) requires a large number of space-varying filters which are very impractical for cost-driven applications.

To address this issue, we apply an approximation model for the space-varying filtering process by taking advantage of the rotational symmetry and the radial correlation of the PSFs across the image field. In essence, we use a linear combination of a small finite set of finite impulse response (FIR) filters (i. e. a filter bank) to represent the radial variation, and use a rotation of these FIR kernels to represent the angular variation. Ideally, the linear space-varying sharpening filters (Wiener filters) for an electro-optical imaging system have the location-dependent spatial frequency response expressed as

$$R_{ideal}(\omega, \nu; m, n) = \frac{P_s(\omega, \nu) H^*(\omega, \nu; m, n)}{P_s(\omega, \nu)|H(\omega, \nu; m, n)|^2 + P_n(\omega, \nu)} \tag{1}$$

where $P_s(\omega, \nu)$ is the power spectral density (PSD) of the original image signal (i.e. ideal image), and $P_n(\omega, \nu)$ is PSD of the noise added to the original image, (ω, ν) are the spatial frequency coordinates,[16] and (m, n) are the pixel locations in the image field. $H(\omega, \nu; m, n)$ is the optical transfer function (OTF) at the field location (m, n). We assume that the additive noise PSD is flat with power σ_n^2 over the entire spectral frequency range. This ideal Wiener filter provides a balanced trade-off between contrast and signal-to-noise-ratio (SNR). We assume a commonly-used signal power spectral density model

$$P_s(\omega, \nu) = \frac{\sigma_s^2}{(1 + c_1^2 - 2c_1(1 - \omega^2))(1 + c_2^2 - 2c_2(1 - \nu^2))} \tag{2}$$

where c_1 and c_2 are image correlation coefficients and σ_s^2 is a parameter which controls the signal power.[16] Here we choose σ_s^2 to achieve the unit signal power.

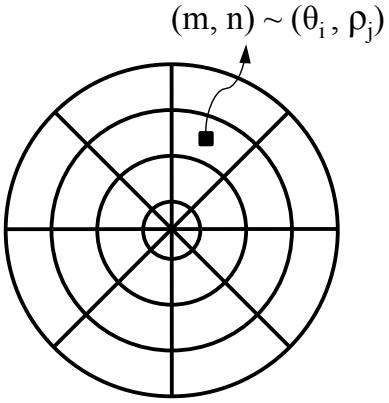

Figure 2. The image field is segmented into a set of polar tiles along the radial and angular dimensions. Each polar tile corresponds to a distinct space-invariant filter.

We now consider the approximation model of the ideal space-varying filters. We first segment the entire image field into a set of polar tiles along the radial and angular dimensions as shown in Figure 2, where each polar tile is represented by an index pair, (θ_i, ρ_j), $i = 0, 1, 2 \ldots, N_\theta$, $j = 0, 1, 2, \ldots, N_\rho$, where N_θ and N_ρ are the predefined angular and radial resolutions, separately. Each polar tile corresponds to a space-invariant filter with distinct frequency response which will be described next. Note that the radial tiling may not be necessarily uniform depending on the target optical system characteristics. Next, given a fixed angular tile index, say $i = 0$, we represent the spatial frequency response of the filter in each radial tile using a linear combination of a small set of filters as follows

$$R(\omega, \nu; \theta_0, \rho_j) = \sum_{k=1}^{K} \alpha_{jk} F_k(\omega, \nu) \tag{3}$$

where K is the predefined total number of the representative filters, i. e. the rank of the filter bank, $F_k(\omega, \nu)$ is the spatial frequency response of the k^{th} filter of the filer bank, and α_{jk} is the weight of the filter kernel for the j^{th} radial tile. The K filter kernels and the associated weights can be optimized using appropriate optimization techniques (e.g. non-convex optimization) and error metric (typically mean squared error (MSE)). For proof of concept for the proposed architecture, we will not discuss the details of the optimization issue in this paper.

Finally, for each angular tile index, i, we represent the spatial frequency response of the filter by rotating the filter at the angle θ_0.

$$R(\omega, \nu; \theta_i, \rho_j) = R(\omega', \nu'; \theta_0, \rho_j) \tag{4}$$

where

$$\begin{bmatrix} \omega' \\ \nu' \end{bmatrix} = \begin{bmatrix} \cos(\Delta\theta_i) & \sin(\Delta\theta_i) \\ \cos(\Delta\theta_i) & -\sin(\Delta\theta_i) \end{bmatrix} \begin{bmatrix} \omega \\ \nu \end{bmatrix}$$

where $\Delta\theta_i = \theta_i - \theta_0$

We will show in the experimental results that this approximation model provides similar level of image quality of the ideal model using small N_θ and K. Next, we will describe the details of the algorithmic framework and hardware architecture based on this approximation model.

3. SPACE-VARYING ROTATION BASED FIR FILTER BANK ARCHITECTURE

Based on the approximation model described in the previous section, we now create a space-varying rotation based FIR filter bank architecture. The essential idea of the space-varying rotation-based FIR filter bank architecture is to rotate the input neighborhood window of the each pixel being processed by a certain angle, and then perform FIR filtering on the rotated input image window using a fixed FIR filter bank adjusted by some weights. The filtering process using such an architecture is an approximation to the ideal space-varying FIR filtering process, providing a tradeoff between complexity and accuracy. The alternative approach would be rotating the FIR filters instead of the input image patch, but this would cause higher complexity of computation due to the multiple rotators required for the FIR filter bank.

Figure 3(a) shows the algorithmic architecture of the proposed space-varying rotation based FIR filter bank. The architecture consists of an input image patch rotator, an FIR filter bank engine, and a controller. The entire input image is processed according to a finite set of predefined polar tiles. In our case, we simply separate the image into N_ρ radial tiles and N_θ angular tiles uniformly. The controller determines the angular index and radial index of the polar tile where the current pixel being processed is located. The angular index determines the amount of the rotation by which the input image patch is rotated by the rotator. The rotated image patch is then filtered with the FIR filter bank, where each FIR filter is adjusted by a weight, which is determined uniquely by the radial index of the current pixel being processed. Figure 3(b) shows the details of the FIR filter bank engine controlled by weights. The FIR filter bank consists of K FIR filter kernels, where K is predetermined. By properly selecting K, where K is always smaller than N_{rho}, the radial correlation of the blur is eliminated. The whole FIR filter bank is designed for a fixed angular location, e.g. 22.5 degree for 8 angular tiles, which should be properly selected to facilitate simple implementation for the radial index computation.

4. HARDWARE IMPLEMENTATION

Figure 4 shows the hardware implementation detail for the overall architecture described in Figure 3. The components are shown as block diagrams. The details are as follows:

4.1 Line Buffer

The left most block shown in the figure is the line buffer. The design of the line buffer on a Xilinx FPGA can incorporate the use of synchronous serial-in serial-out shift registers in slices (SRL16) or can be designed using block RAMs. The design with block RAMs uses a counter to address the memory. The block RAMs used are of type **read first**. A read frame is a virtually defined window of pixels which is equal to $\sqrt{2}F_h \times \sqrt{2}F_w$ where F_h and F_w are the maximum height and width of the filters in the P-Filter Bank. These number of bits are chosen at a time to be processed by the rotator and provide the filter with the relevant bits to perform the filtering (sharpening) for the pixel under process.

4.2 Pre-buffer

The pre-buffer block which is built using parallel in - parallel out registers. These are LUTs since SRL16s cannot be inferred on the Xilinx fabric for parallel in operation.

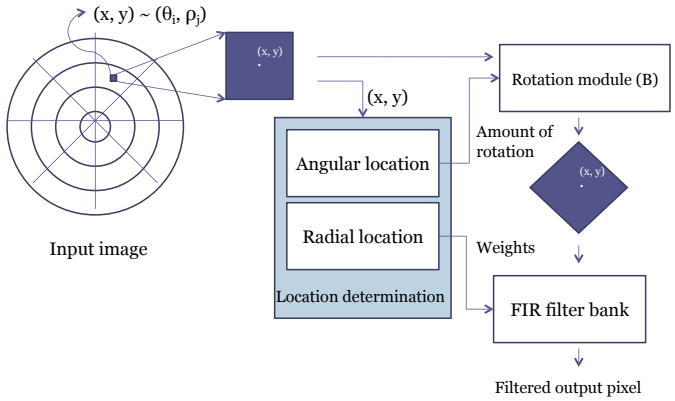

(a) Structure of the rotation-based FIR filter bank

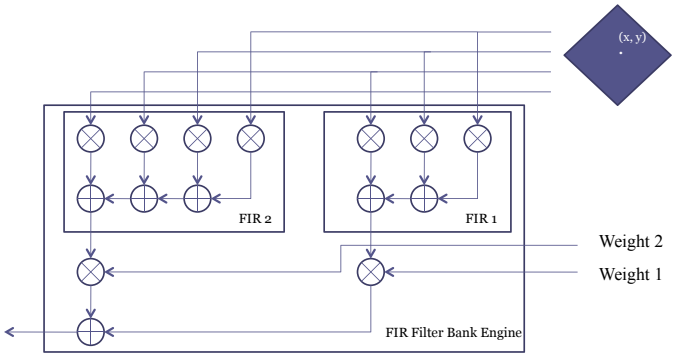

(b) The FIR filter bank controlled by weights

Figure 3. The diagram shows the algorithmic architecture of the space-varying rotation-based FIR filter bank. (a) shows the overall structure of the rotation-based filter bank. The architecture includes an input image patch rotator followed by an FIR filter bank engine, and a controller which determines the angular and radial locations of the current pixel being processed. (b) shows the details of the FIR filter bank engine controlled by weights. The weights are determined by the radial location of the current pixel.

4.3 Rotator:

Figure 5 illustrates the rotator structure using multi-stage multiplexers. The structure consists of three stages of binary multiplexers, where the output of each stage switches between the zero degree input and the rotated value at a basis rotation angle. Each multiplexer is controlled by the control bit of the corresponding rotating angle. The three-stage multiplexer network can be used for 8 rotation angles: 0, 45, 90, 135, 180, 225, 270, and 315 degree, each of which is enabled by a different set of three control bits. For example, if the rotation angle is 135 degree, the control byte created from the rotation angle generator is 110, where each bit from the MSB to LSB controls the 45, 90, and 180 degree multiplexers, separately. In this case, the 45 and 90 degree multiplexers are enabled, and the 180 degree multiplexer is disabled, therefore producing an 135 degree rotation at the output. The rotation indices of the input image patch at difference angles are created by using the nearest neighbor interpolation method in Matlab at the design time. The effect of the interpolation error on the filtering result varies with the rotation angles. This effect is demonstrated in the simulated results in Sectioin 5.

4.4 Filter Bank

The P-Filter Bank consists of a set of P filters which can be designed as Multiply-and-Accumulate (MAC), Distributed Arithmetic (DA) or Shift-and-Add. These architectures are well documented in the literature.

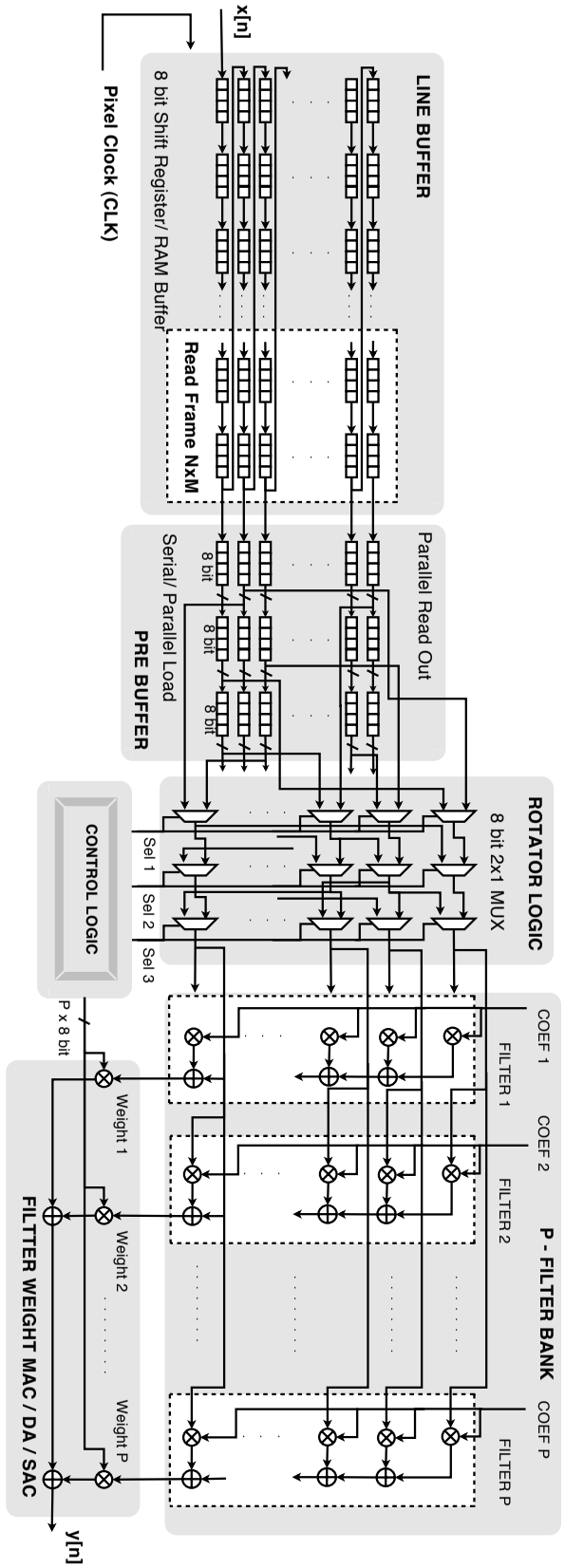

Figure 4. FPGA hardware design for the architecture shown in Figure 3

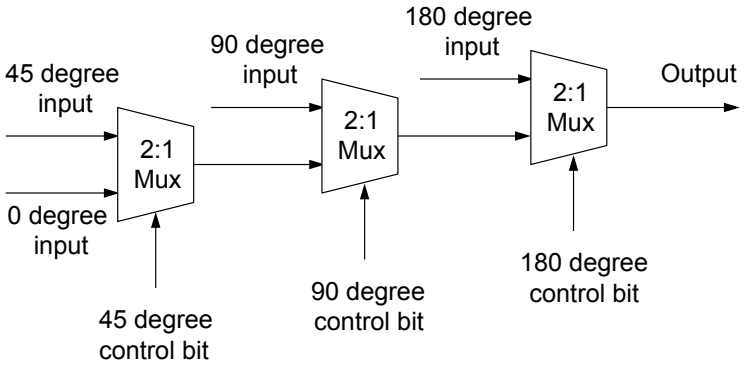

Figure 5. This diagram illustrates the rotator structure using multi-stage multiplexers (Mux). The structure consists of three stages of binary multiplexers, where the output of each stage switches between the zero degree input and the rotated value at a basis rotation angle. Each multiplexer is controlled by the control bit of the corresponding rotating angle. The three-stage multiplexer network can be used for 8 rotation angles: 0, 45, 90, 135, 180, 225, 270, and 315 degree, each of which is enabled by a different 3-bit control signal.

4.5 Filter Weight MAC

This block weights the filter outputs using some predefined weights. The weights are determined from the control logic block based on the radial tile to which the current pixel belongs.

4.6 Control Logic

The controller generates the selecting signals for the multiplexer rotator and the weights to be assigned to the filter bank based on the radial tile index of the current pixel. It consists of five major parts: coordinate counter that outputs the X and Y coordinate values, linear function computation that detects the angular tile boundaries, rotation Index block that computes the angular position of the current pixel, radius square (ρ^2) generator that computes radius value of the current pixel, and radial index block that computes the radial location of the current pixel, and selects the associated set of weights for further filter bank computation

5. EXPERIMENTAL RESULTS

In our experiment, we simulate the deblurring results by applying the space-varying rotation based FIR filter bank for an optical system having large lateral color aberrations. The goal of this experiment is to analyze the image quality performance of the space-varying rotation based FIR filter results by comparing with the results using ideal space-varying Wiener filters. For both filtering processes, we use 10 radial tiles and 8 angular tiles, which are all uniformly segmented over the entire image. The FIR filter bank used in the experiment includes only two FIR filters, one is a 5×5 rotationally symmetric FIR filter, and another one is a 5×9 rotationally asymmetric FIR filter. For simplicity, these two kernels are not optimized, instead they are set to be the FIR Wiener filters designed for the image center and the outer polar tile on the image edge, separately. The weights of the two filter kernels for each radial tile are simply determined by the cubic function of the radius.

Figure 6 shows the comparison of the simulation results for two different sharpening filtering approaches: the ideal space-varying Wiener filters and the space-varying rotation based FIR filter bank using 2 kernels. Figure 6(b) shows the the captured image which is unprocessed. Figure 6(c) shows the ideal space-varying Wiener filter result obtained by applying a distinct IIR Wiener filter to each polar tile defined by the 10 radial tiles and 8 angular tiles. Figure 6(d) shows the space-varying rotation based FIR filter bank result by using 2 FIR filter kernels with 8 rotation angles. The results demonstrate that the quality of the image processed by the 2-kernel space-varying rotation based FIR filter bank is close to that of the image processed by the ideal space-varying Wiener filters, where both methods produce similar sharpness around edges.

We perform exhaustive experiments for analyzing the implementation complexity of the proposed architecture on a Xilinx Spartan-3E FPGAs. We test a set of 2-kernel and 3-kernel FIR filter banks with various filter sizes. The input image is set to VGA (640×480) and 8-bit depth. We define the polar tiles by separating the entire image into 8 angular tiles and 10 radial tiles uniformly. The coefficient bit precision of each filter kernel is set to be 12 bits.

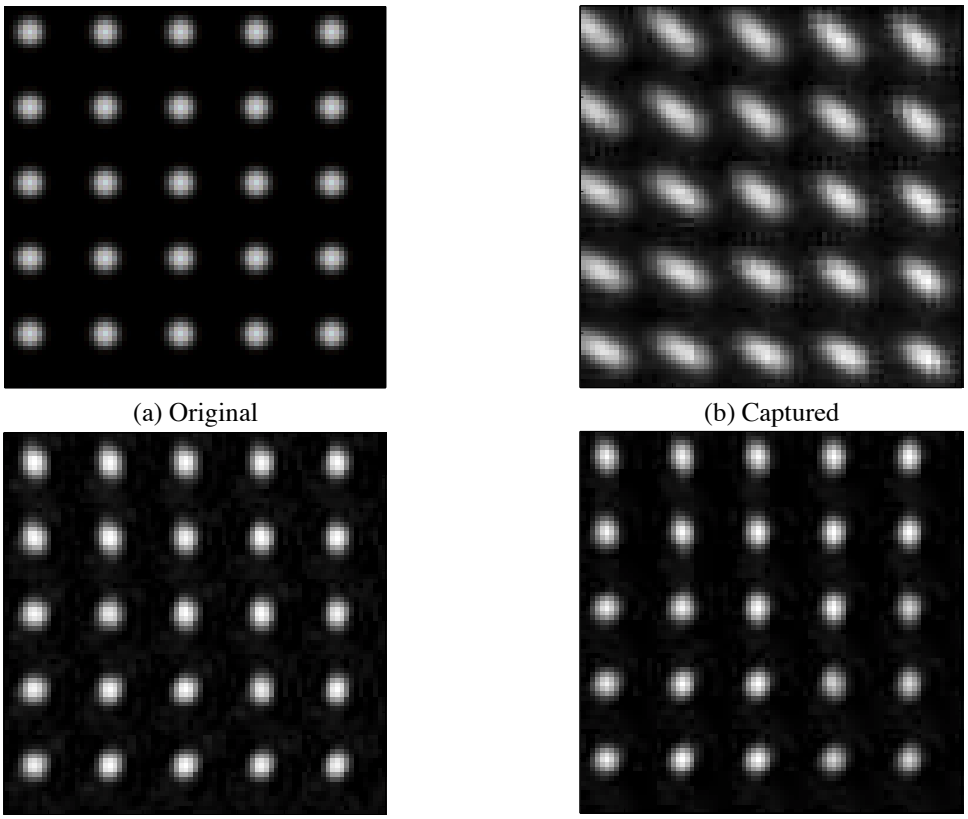

(a) Original (b) Captured

(c) Ideal space-varying Wiener filters (d) Space-varying rotation based 2-kernel FIR filter bank

Figure 6. The figure shows the simulated results for two different sharpening filtering approaches. (a) shows the original (ideal) image. (b) shows the unprocessed captured image. (c) shows the image processed by ideal space-varying Wiener filters. (d) shows the image processed by the rotation-based FIR filter bank using 2 FIR filter kernels and 8 rotation angles.

A major challenge in the design of the space-varying filter was to assess its feasibility on a low-end FPGA like Xilinx Spartan-3E. In this section, we present implementation results and observe that the occupied area (number of slices) for the design is practical. Figure 7 and Figure 8 show the number of occupied slices and LUTs for the space-varying rotation-based FIR filter architecture containing the 2-kernel and 3-kernel FIR filter banks, separately, versus the number of filter taps. The number of filter taps is the total of the taps of all the kernels in the filter bank. For example, for a 2-kernel filter bank containing a 5×5 and a 7×11 kernel, the total number of the filter taps is $5 \times 5 + 7 \times 11 = 102$. Note that there are a few bumps in the figures, where the occupied area decreases by a small number when the filter tap number increases. This is due to the fact that the complexity of the space-varying rotator is a function of maximum width and height of the filter bank kernels, but is not directly dependent on the total number of filter taps.

Figure 9 and Figure 10 show the minimum clock periods for the space-varying rotation-based filter architecture containing the 2-kernel and 3-kernel FIR filter banks, separately, versus the number of filter taps. Pipelining techniques could be used efficiently for achieving the desired clock frequency. The complexity optimization for the pipelined architecture is a design problem and is addressed using many techniques detailed in the literature.[17]

6. CONCLUSIONS

We have presented a novel low-cost space-varying FIR filter architecture suitable for jointly designed computational imaging systems. We achieve the low cost by taking advantages of the correlation of both the radial and angular properties of the target optical systems. We show that the implementation of this architecture is feasible on the low-end Xilinx FP-

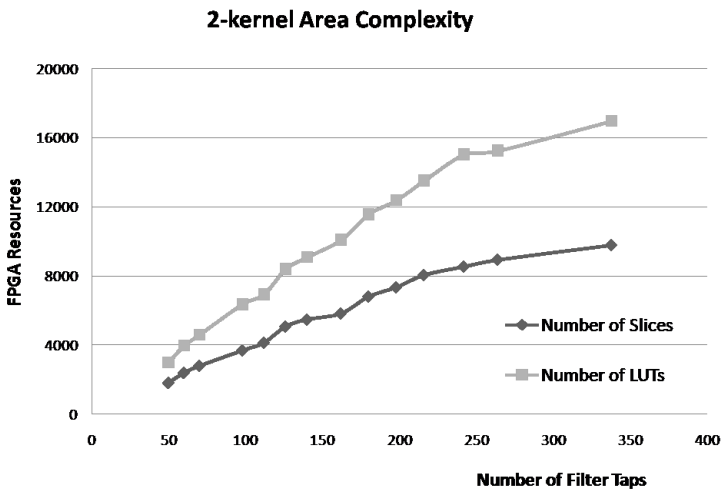

Figure 7. Two kernel implementation - area occupied

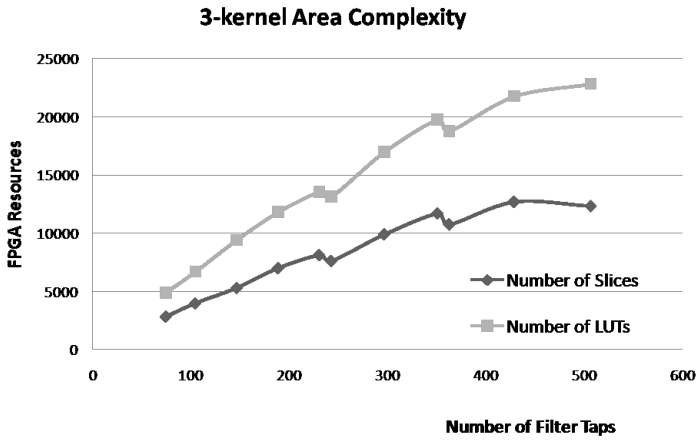

Figure 8. Three kernel implementation - area occupied

GAs. In addition, we want to emphasize that this architecture could also be a feasible low-cost solution on ASIC or SOC (system-on-chip).

REFERENCES

[1] Dowski, E. and Cathey, W. T., "Extended depth of field through wave-front coding," *Applied Optics* **41**, 1859–1866 (1995).

[2] George, N. and Chi, W., "Extended depth of field using a logarithmic asphere," *Journal of Optics A: Pure Applied Optics* **5**(5), S157–S163 (2003).

[3] Mouroulis, P., "Depth of field extension with spherical optics," *Optics Express* **16**(17), 12995–13004 (2008).

[4] Stork, D. G. and Robinson, M. D., "Theoretical foundations for joint digital-optical analysis of electro-optical imaging systems," *Applied Optics* (April 2008).

[5] Robinson, M. D. and Stork, D. G., "Joint design of lens system and digital image processing," in [*Proceedings of the International Optical Design Conference*], Gregory, G., Howard, J., and Koshel, J., eds., **6342**, OSA (August 2006).

[6] L, S., "Use of a sharpness criterion in correcting images degraded by random distortion," *Journal of The Optical Society of America A: Optics and Image Science* **5**, 1492–1501 (1988).

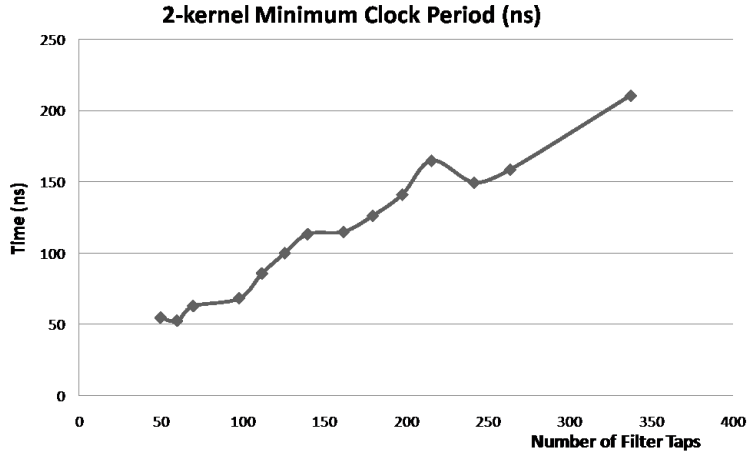

Figure 9. Two kernel implementation - minimum clock period

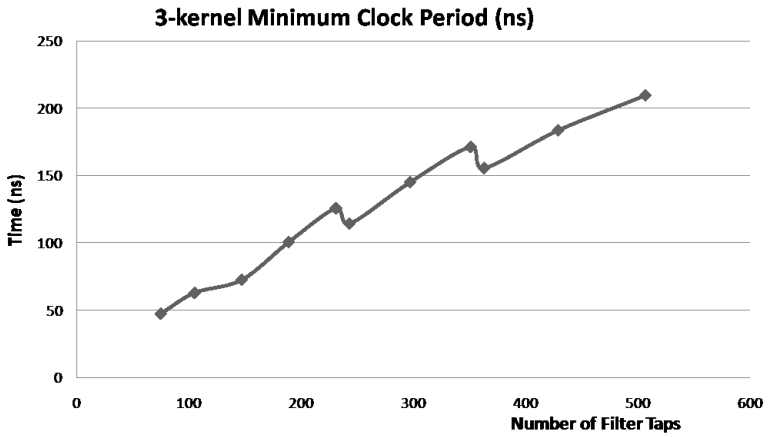

Figure 10. Three kernel implementation - minimum clock period

[7] Nagy, J. G. and OLeary., D. P., "Iterative image restoration using approximate inverse preconditioning," *F. T. Luk, ed., Advanced Signal Processing Algorithms, Architectures, and Implementations IV* **3162**, 388–399 (1997).

[8] Nagy, J. G. and OLeary., D. P., "Restoring images degraded by spatially-variant blur," *SIAM Journal on Scientic Computing* **19**, 1063–1082 (1998).

[9] Adorf, H.-M., "Towards hst restoration with a space-variant psf, cosmic rays and other missing data," *The Restoration of HST Images and Spectra II, R. J. Hanisch and R. L. White, eds., Space Telescope Science Institute, Baltimore, MD* , 72–78 (1994).

[10] Hanke, M. and Hansen, P. C., "Regularization methods for large-scale problems," *Surveys Math* **3**, 253–315 (1993).

[11] McNown, S. R. and Hunt, B. R., "Approximate shift-invariance by warping shift variant systems," *The Restoration of HST Images and Spectra II, R. J. Hanisch and R. L. White, eds., Space Telescope Science Institute, Baltimore, MD* , 181–187 (1994).

[12] Sawchuk, A. A., "Space-variant image restoration by coordinate transformations," *Proceedings of the IEEE* **60**, 854–864 (July 1972).

[13] Trussel, H. J. and Hunt, B. R., "Image restoration of space variant blurs by sectional methods," *Proceedings of the IEEE Transactions on Accoustic Speech Signal Processing* **ASSP-26**, 608–609 (1978).

[14] Trussel, H. J. and Fogel, S., "Identification and restoration of spatially variant motion blurs in sequential images," *Proceedings of the IEEE Transactions on Image Processing* **1**, 123–126 (Jan 1992).

[15] Tekalp, A. M., Kaufman, H., and Woods, J. W., "Model-based segmentation and space-variant restoration of blurred images by decision-directed filtering," *Elsevier Signal Processing* **15**(3), 259–269 (1988).

[16] Jain, A. K., [*Fundamentals of Digital Image Processing*], Prentice Hall, Englewood Cliffs, New Jersey, 1 ed. (1989).

[17] Andres. D. Garcia, Jean Luc Danger, W. B., "Low power digital design in FPGAs: A study of pipeline architectures implemented in an FPGA using a low supply voltage to reduce power consumption," *International ACM Symposium on Field-Programmable Gate Arrays* **0**, 220–220 (2000).